DROOP CONTROL OF RENEWABLE ENERGY DISTRIBUTION GENERATION IN DC MICROGRID

Swarupa.V[1], Abdul Nadeem MD[2]

[1] *Student, Electrical and Electronics Engineering, Nigama Engineering College, Telangana, India*
[2] *Asst.Prof, Electrical and Electronics Engineering, Nigama Engineering College, Telangana, India*

ABSTRACT

This paper presents analysis of power flow management in wind power and wave power. This paper proposed an integrated wind and wave power generation system fed to an ac power grid or connected with an isolated load using a dc microgrid. The proposed dc microgrid connects with a wind power generator through a voltage-source converter (VSC), a wave power generator through a VSC, an energy storage battery through a bidirectional dc/dc converter, a resistive dc load through a load dc/dc converter, and an ac power grid through a bidirectional grid-tied inverter. The studied integrated wind and wave system joined with the dc microgrid is modeled and simulated using MATLAB/Simulink model design reveals that the proposed integrated control system can maintain stable operation to supply power under different operating conditions using the proposed dc microgrid by varying duty ratios of individual converter and pitch angle of wind system is shown.

Keyword: *- Wind power, Wave power, Droop control, Battery storage, Micro grid*

---

1. INTRODUCTION

Renewable energy and distributed generation systems (DGSs) have attracted increasing attention and have been extensively researched and developed. They gradually alter the concepts and operations of conventional power generation systems. The rise in several countries makes it possible that this kind of DGS can be practically applied to a grid-tied system or an isolated system with wind power, solar energy, hydropower, etc. The output of DGS usually includes two kinds: dc and variable ac. Moreover, the generating capacity of DGS comparing with conventional large synchronous generators is much smaller, and hence, the dc microgrid can be practically applied to convert the generated time-varying quantities of natural renewable energy and DGS into smooth dc electricity that can then be converted back into ac quantities delivered to other power systems [1], [2]. Because of the intermittence of renewable energy and DGS, bidirectional dc/dc converters are usually necessary to feed the connected loads with smooth power [3].

In order to simulate a hybrid ac/dc microgrid system, photovoltaic and wind power generator models, a doubly fed induction generator model, and an inverter model were established to simulate the dynamic responses of the studied system in [4]. A practical low-voltage bipolar-type dc microgrid was constructed using a gas engine as the power source, while a bidirectional dc/dc converter shunting a super capacitor was utilized as an energy storage device to balance the power demand of the studied system in [5]. Unexplored energy and resources in ocean such as marine energy, tidal energy, ocean thermal energy, ocean wave energy, salinity gradient energy, etc., are abundant. The simulated results of an Archimedes wave swing (AWS) power convertor coupling with a linear permanent magnet generator (LPMG) were simulated using MATLAB/Simulink. A configuration of a marine power plant with two AWSs connecting to a power grid was proposed in [7], and the outputs of the two AWSs were converted to dc quantity by individual diode bridge rectifiers and then subsequently converted into ac quantity by an inverter to reduce the fluctuation of the combined rectified output power.

A hybrid electric vehicular power system in [8] utilized two motors connected to a dc bus through a voltage-source converter (VSC), and a bidirectional converter was connected between a battery and the dc bus. The dynamic average model was used in [8] for all power electronics models by neglecting the switching phenomena

to reduce simulation computational intensity. A non isolated bidirectional zero-voltage switching dc/dc converter was proposed in [9], and the converter utilized a very simple auxiliary circuit consisting of an additional winding of a main inductor and an auxiliary inductor to reach zero voltage switching and reduce the reverse-recovery problem of power diodes.

Modeling and testing the data centers of a dc microgrid using MATLAB were proposed in [10] and [11] since most data centers were sensitive to the variations of electronic loads. The proposed dc microgrid was also used to supply sensitive electronic loads during ac grid outages in order to offer uninterruptible power system protection [11]. To achieve power sharing and improve economic benefit, a dc bus voltage control technique for parallel integrated permanent magnet wind power generation systems was proposed in [12], and the technique was based on a master–slave control to solve controller discrepancy problems. In order to achieve power sharing and to optimize the dc microgrid, the control strategies for an islanded microgrid with a dc-link voltage control were developed in [13] and [14], while the control strategies were combined with P/V droop control and constant-power band to avoid frequent changes and voltage-limit violation on generation devices.
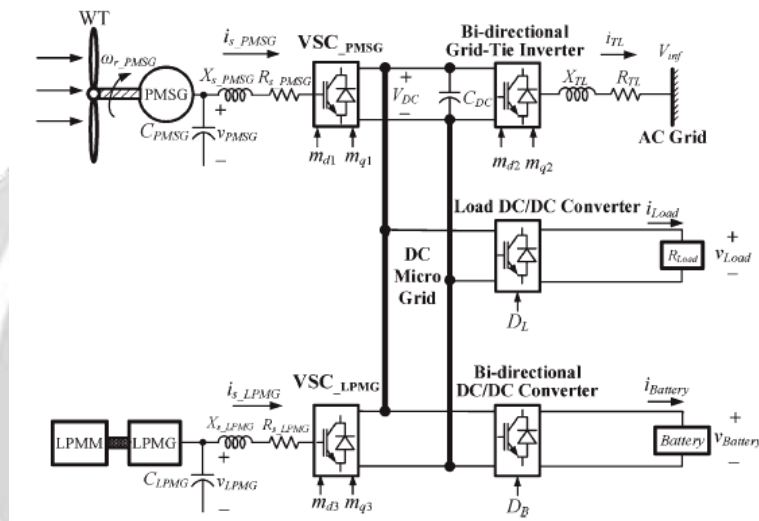
Fig-1: Configuration of the studied integrated wind and wave power generation system connected to a power grid through the proposed dc microgrid.

A battery/ultra capacitor hybrid energy storage system was proposed in [15] for electric-drive vehicles. To satisfy the peak power demands between the ultra capacitor and battery, a larger dc/dc converter was necessary. The studied system utilized two storage devices to compensate mutually in order to prolong the life of the battery. The simulated and experimental results were carried out to verify the proposed control system. This paper proposes an integrated wind and wave power generation system fed to a power system or connected with an isolated load using a dc microgrid. A bidirectional dc/dc converter is proposed to achieve the integration of both wind and wave power generation systems with uncertainty and intermittent characteristics.

2. DESIGN OF A WIND TURBINE GENERATING SYSTEMS

The realization of a wind turbine as a source of clean, non-polluting and renewable energy may depend on the optimum design of the system and the control strategies of the different possible parameters that can operate efficiently under extreme variations in wind conditions. The general goal of this paper is to optimize the electromechanical energy conversion of the wind turbines, developing suitable strategies of control. Both induction and synchronous generators can be used for wind turbine systems. Mainly, three types of induction generators are used in wind power conversion systems: cage rotor, wound rotor with slip control and doubly fed induction rotors. The last one is the most utilized in wind speed generation because it provides a wide range of speed variation. However, the variable-speed directly-driven multi-pole permanent magnet synchronous generator (PMSG) wind architecture is chosen for this purpose and it is going to be modeled: it offers better performance due to higher efficiency and less maintenance because it does not have rotor current. What is more, PMSG can be used without a gearbox, which implies a reduction of the weight of the nacelle and reduction of costs.

2.1. System Modeling

Topology of non-grid-connected wind energy conversion system this paper discussed is shown in Fig.1. PMSG that with PWM voltage source vector control which can enable a high energy efficiency by adjusting the rotational speed, is directly driven by a fixed pitch wind turbine, DC bus voltage is constant under the control of Boost converter which ensures the power balance of the system, Buck converter is introduced to maintain the output voltage a constant. The basic control strategy is to achieve maximum peak power tracking of wind turbine while operating in below rated power condition and to limit the power while operating in the above rated power condition.
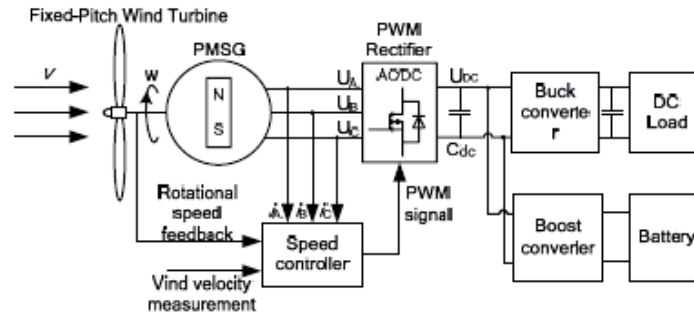
Fig-2: Topology of non grid connected wind energy conversion system

2.2 Wind Turbine

1.   Generator Model
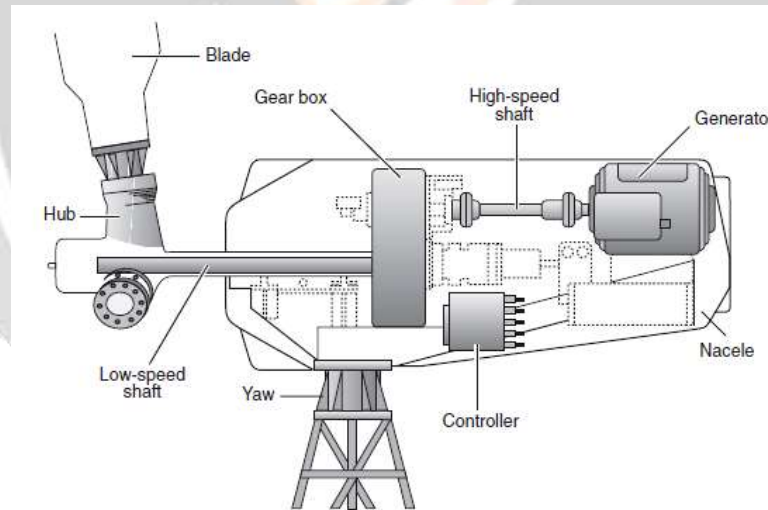
Fig-3: Horizontal axis wind mill

The wind systems that exist over the earth's surface are a result of variations in air pressure. These are in turn due to the variations in solar heating. Warm air rises and cooler air rushes in to take its place. Wind is merely the movement of air from one place to another. There are global wind patterns related to large scale solar heating of different regions of the earth's surface and seasonal variations in solar incidence. There are also localized wind patterns due the effects of temperature differences between land and seas, or mountains and valleys. Wind speed generally increases with height above ground. This is because the roughness of ground features such as vegetation and houses cause the wind to be slowed.

In the wind turbine the first system is calculated by:

$$\lambda = \frac{R\omega}{v} \qquad \text{............ (1)}$$

Cp value is calculated in the next subsystem by using the following formula:

$$C_p(\lambda, \vartheta) = c_1 \left(c_2 \frac{1}{\beta} - c_3\vartheta - c_4\vartheta^x - c_5 \right) e^{-c_6\frac{1}{\beta}} \qquad \text{............ (2)}$$

$$J\frac{d\omega}{dt} = T_m - T_{em} - F_w \qquad \text{............ (3)}$$

J: Inertia moment of the turbine, axle and generator

F: Axle friction

Tem: Electromagnetic torque

Wind speed data can be obtained from wind maps or from the meteorology office. Unfortunately the general availability and reliability of wind speed data is extremely poor in many regions of the world. However, significant areas of the world have meant annual wind speeds of above 4-5 m/s (meters per second) which makes small-scale wind powered electricity generation an attractive option. It is important to obtain accurate windspeed data for the site in mind before any decision can be made as to its suitability. Methods for assessing the mean wind speed are found in the relevant texts (see the 'References and resources' section at the end of this fact sheet).

The power in the wind is proportional to:

• The area of windmill being swept by the wind

• The cube of the wind speed

• The air density - which varies with altitude

The formula used for calculating the power in the wind is shown below:

$$\text{Power} = \frac{\text{density of air x swept area x velocity cubed}}{2}$$
$$P = \frac{1}{2}\rho A V^3$$

Where, P is power in watts (W)

   ρ is the air density in kilograms per cubic metre (kg/m3)

   A is the swept rotor area in square metres (m2)

   V is the windspeed in metres per second (m/s)

The fact that the power is proportional to the cube of the wind speed is very significant. This can be demonstrated by pointing out that if the wind speed doubles then the power in the wind increases by a factor of eight. It is therefore worthwhile finding a site which has a relatively high mean wind speed.

2.3 Fixed- Pitch Wind Turbine Model

The kinetic energy of the wind (air mass m, wind speed v) is given by the following equation:

$$E_c = \frac{1}{2}mv^2 \qquad \text{............ (4)}$$

With: $m = \rho v S \Delta t$

(With S: Covered surface of the turbine and p: the air density)

The wind power has the following expressions:

$$P_w = \frac{d}{dt} E_c \Rightarrow P_w = \frac{1}{2}\rho S v^3 \quad \ldots\ldots\ldots \quad (5)$$

The mechanical power that the turbine extracts from the wind is inferior to . This is due to the fact that the wind speed after the turbine isn't zero (the air needs to be carried off after the turbine). So, the power coefficient

of the turbine can be defined by:

$$C_p = \frac{P_m}{P_w}; \quad C_p < 1 \quad \ldots\ldots\ldots \quad (6)$$

The recuperated power is given by:

$$P_m = \frac{1}{2}\rho \pi R^2 v^3 C_p \quad \ldots\ldots\ldots \quad (7)$$

With R: radius of the rotor.

Cp depends of the tip speed ratio of the wind turbine

,β angle of the blades.

$$C_p = C_p(\lambda, \beta) \quad \text{With: } \lambda = \frac{R\omega}{v} \quad \ldots\ldots\ldots \quad (8)$$

is the rotation speed of the rotor.

A maximum for this function can be found and this maximum is known as the limit of Betz:

$$C_{pmax} = \frac{16}{27} = 0{,}593 \quad \ldots\ldots\ldots \quad (9)$$

The wind turbine torque on the shaft can be calculated from the power:

$$T_m = \frac{P_m}{\omega} = \frac{1}{2}\rho \pi R^2 \frac{v^3}{\omega} C_p \quad \ldots\ldots\ldots \quad (10)$$

$$T_m = \frac{1}{2}\rho \pi R^3 v^2 C_T \quad \ldots\ldots\ldots \quad (11)$$

2.4 PERMANENT MAGNET SYNCHRONOUS GENERATOR MODEL

The PMSG is modeled under the following simplifying assumptions: sinusoidal distribution of stator winding, electric and magnetic symmetry, negligible iron losses and unsaturated model in the so-called steady-state (or stator) coordinates is first obtained. Another simpler model can be obtained in (d,q) rotor coordinates, conversion between (a,b,c) and (d,q) coordinates can be realized by means of the Park Transform. Then, after neglecting the homopolar voltage, $u0$, by virtue of symmetry, the (d,q) PMSG model becomes .

$$\begin{cases} u_d = R i_d + L\dfrac{di_d}{dt} - p\omega i_q \\[2mm] u_q = R i_q + L\dfrac{di_q}{dt} + p\omega i_d + p\psi_f \omega \\[2mm] T_e = \dfrac{3}{2} p\psi_f i_q \end{cases}$$

where *R* is the stator resistance, ud, uq are d and q stator voltages, id, iq are d and q stator currents, *p* is the number of pole pairs, f is the flux that is constant due to permanent magnets, as the permanent magnets are mounted on the rotor surface, d, q inductances are equal, they are represented as *L*. By introducing the coordinate transformation, electromagnetic torque is only determined by iq, which highly simplifies the controller design of PMSG.

3. MODELLING OF THE PROPOSED SYSTEM

3.1 Overview of System Configuration

Fig. 1 shows the configuration of the studied integrated wind and wave power generation system connected to an ac grid through a dc microgrid. The wind power generation system simulated by a permanent-magnet synchronous generator (PMSG) driven by a wind turbine (WT) is connected to the dc microgrid through a VSC of VSC_PMSG.
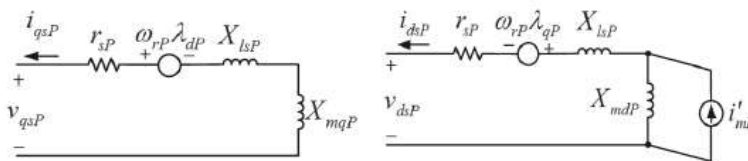
Fig-4: q-d axis equivalent circuit model of the studied wind PMSG

The wave power generation system simulated by an LPMG driven by a linear permanent magnet motor (LPMM) is also connected to the dc microgrid through a VSC of VSC_LPMG. A resistive dc load *R*-Load is connected to the dc microgrid through a load dc/dc converter. To achieve stable power flow (or power balance condition) and load demand control of the dc microgrid under different operating conditions, a battery is connected to the dc microgrid through a bidirectional dc/dc converter, while an ac grid is connected to the dc microgrid through a bidirectional grid-tied inverter and a transmission line. When available wind power and/or wave power can be injected into the dc microgrid with a fully charged battery, the surplus power of the dc microgrid can be delivered to the ac grid through the bidirectional grid-tied inverter. When no wind power or no wave power is delivered to the dc microgrid with a low-energy battery, the insufficient power of the dc microgrid can be captured from the ac grid through the bidirectional grid-tied inverter.

The power of the resistive dc load *R*-Load can be obtained from the dc microgrid through the load dc/dc converter only when the dc microgrid has enough power. The load dc/dc converter with the resistive dc load *R*-Load can also slightly adjust the power balance condition of the dc microgrid. The control functions of the bidirectional dc/dc converter, the bidirectional grid-tied inverter, and the load dc/dc converter must be adequately coordinated with each other to obtain stable operation of the dc microgrid. In this thesis, the mathematical models of the studied integrated system with the proposed dc microgrid are derived in detail, including the wind WT-PMSG set with its VSC, the wave LPMM-LPMG set with its VSC, the bidirectional dc/dc converter with the battery, the load dc/dc converter with the resistive load, and the bidirectional grid-tied inverter. Both frequency-domain analysis and time-domain simulations are performed using MATLAB/Simulink.

4. EQUIVALENT MODELS

4.1 Equivalent Models of Wt and Pmsg

The WT model employed in this paper includes the following operation conditions: the cut-in wind speed of 4 m/s, the rated wind speed of 13 m/s, and the cut-out wind speed of 24 m/s. The detailed characteristics and expressions for the captured mechanical power *Pw*, the dimensionless power coefficient *Cpw*, the mechanical torque *Tw*, the tip speed ratio *λw*, and the blade pitch angle *βw* of the studied WT can be seen. Fig. 4.1 plots the *q*–*d*-axis equivalent circuit of the studied wind PMSG. The per-unit (p.u.) *q*- and *d*-axis stator winding voltages of the studied PMSG can be expressed by equation as follows are the *q*- and *d*-axis stator-winding magnetic fluxes, respectively

$$v_{qsP} = -r_{sP}i_{qsP} + p(\lambda_{qP})/\omega_b + \omega_{rP}\lambda_{dP}/\omega_b \quad \ldots\ldots\ldots \quad (13)$$

$$v_{dsP} = -r_{sP}i_{dsP} + p(\lambda_{dP})/\omega_b - \omega_{rP}\lambda_{qP}/\omega_b$$

where

$$\ldots\ldots\ldots \quad (14)$$

$$\lambda_{qP} = -(X_{mqP} + X_{lsP})i_{qsP}$$
$$\lambda_{dP} = -(X_{mdP} + X_{lsP})i_{dsP} + X_{mdP}i'_{mP}$$

$i_{qs}P$ and $i_{ds}P$ are the q- and d-axis stator-winding currents, respectively; $X_{mq}P$ and $X_{md}P$ are the q- and d-axis magnetizing reactance's, respectively; $X_{ls}P$ is the leakage reactance; $X_{m}P$ is the magnetizing current; r_sP is the stator winding equivalent resistance; and ω_rP is the rotor speed of the studied PMSG, while p is the differential operator with respect to time t (i.e., p = d/dt), and ωb is the base angular speed in radians per second.

4.2 Equivalent Models Of Aws And Lpmg

The AWS utilizes the wave swing to drive the generator to produce electric power without transmission medium. The motion of the AWS in fluid is affected by the damping force and spring force. The equivalent mass-spring-damper model of the studied AWS is illustrated, whose motion equations can be described by

$$p(z) = u \qquad\qquad \text{............ (15)}$$
$$(m)p(u) = F_{\text{wave}} - (S)z - (D)u$$

where *m* is the sum of the masses of the floater and the LPMG translator; *D* and *S* are the damping coefficient and spring constant, respectively; and F_{wave}, *z*, and *u* are the floater driving force, distance traveled by the floater, and speed of the floater of the AWS, respectively [18]–[21]. Fig. 4.2 draws the *q–d*-axis equivalent circuit model of an LPMG. The nonlinear p.u. differential equations of the LPMG can be written as

$$(X_q)p(i_{qsg}) = -v_{qsg} - Ku_s X_{mdg}i_{qsg}$$
$$\qquad\qquad - R_{sg}i_{qsg} + Ku_s X_{mdg}i'_{mg}$$
$$(X_d)p(i_{dsg}) = -v_{dsg} + Ku_s X_{mqg}i_{qsg} - R_{sg}i_{dsg}$$

where *idsg* and *iqsg* are the d- and q-axis equivalent magnetizing currents, respectively; *Xmg* is the magnetizing current; *Xlsg* is the equivalent leakage reactance; *Rsg* is the equivalent internal resistance; *Xmqd* and *Xmdg* are the q- and d-axis magnetizing inductance, respectively; and *Xd = Xlsg + Xmdg* and *Xq = Xlsg + Xmqg* of the studied LPMG, while *K = π/τp, τp* is the electrode distance, and *us* is the forcer movement speed of the LPMG.

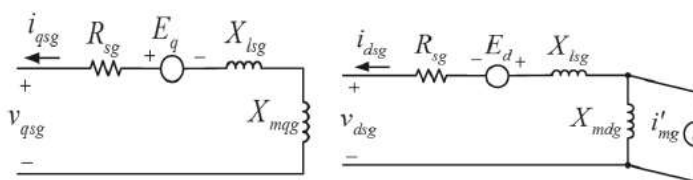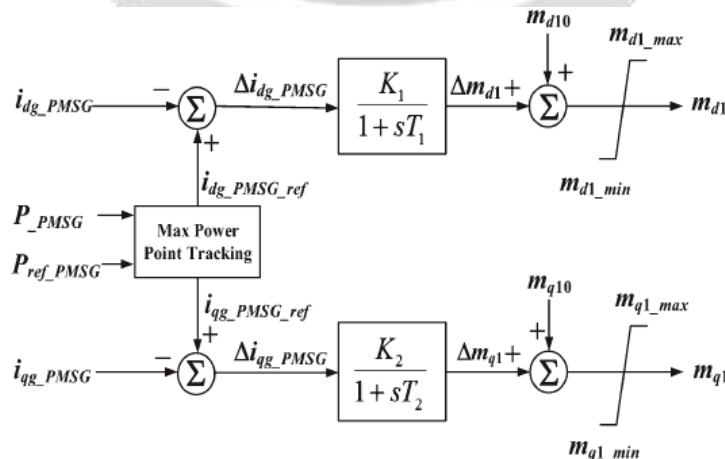**Fig-5:** *q–d*-axis equivalent circuit model of the studied LPMG.

Fig-6: Control block diagram of the modulation indices of the VSC of the studied PMSG.

4.3 DESIGN OF CONTROL BLOCKS OF PMSG'S VSC

Fig. 4.3 illustrates the control block diagrams of the indices $mq1$ and $md1$ of the studied PMSG's VSC. The d- and q-axis reference currents are generated by comparing the output active power of the PMSG ($PPMSG$) with its reference value using maximum power point tracking function. After subtracting the output currents of the PMSG (ig_PMSG) from their respective reference values, the resultant differences pass through the respective first-order lag controllers to obtain the deviations of the respective modulation indices that are added to their respective initial values to acquire the VSC's modulation indices. The limiters, namely, $md1$_max, $md1$_min, $mq1$_max, and $mq1$_min, are included in the model to ensure normal operation of the VSC.

4.4 CONTROL BLOCKS OF LMSG'S VSC

Fig. 4.4 plots the control block diagrams of the indices $mq3$ and $md3$ of the studied LPMG's VSC. After subtracting the output currents of the LPMG (ig_LMSG) from their respective reference values, the resultant differences pass through the respective proportional-integral controllers to obtain the deviations of the respective modulation indices which are added to their respective initial values to obtain the VSC's modulation indices. The limiters, namely, $md3$_max, $md3$_min, $mq3$_max, and $mq3$_min, are included in the model to ensure normal operation of the VSC.

4.5 CONTROL BLOCKS OF BIDIRECTIONAL GRID-TIED INVERTER

Fig. 4.5 draws the control block diagram of the modulation indices $mq2$ and $md2$ of the grid-tied voltage-source inverter (VSI). The grid-tied VSI is required to feed the generated power of the renewable-energy systems to the power grid.
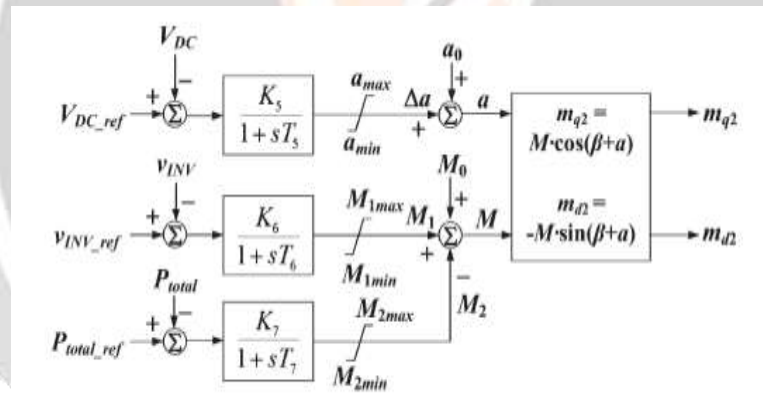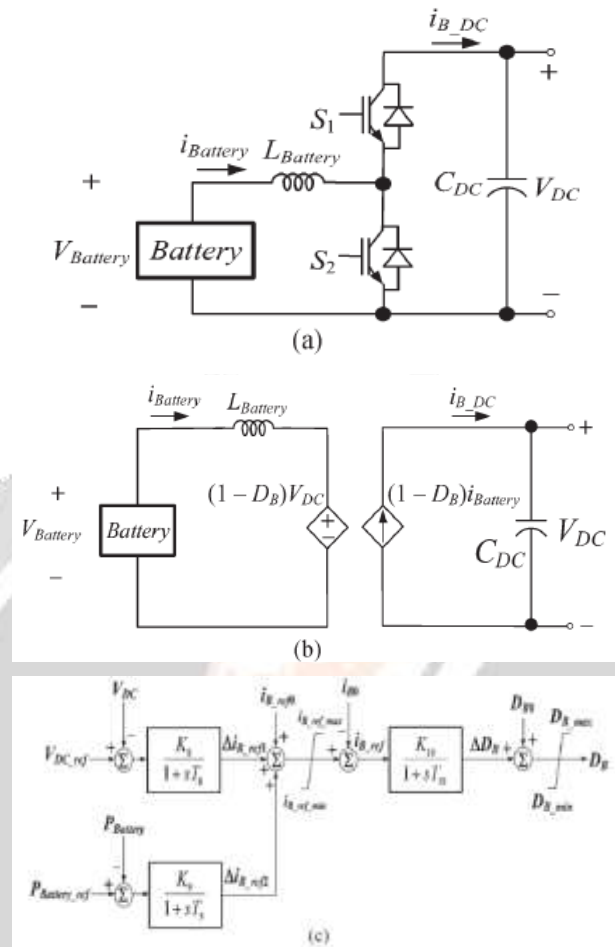

Fig-7: control block diagram of the modulation indices of grid VSI

4.6 MODEL OF BIDIRECTIONAL DC/DC CONVERTER

Fig. 4.6 (a) shows the basic schematic diagram of the employed bidirectional dc/dc converter with a synchronous-buck structure. The converter consists of two power switches ($S1$ and $S2$) and an energy-store inductance $L_{Battery}$. The design purpose of this converter is that the energy storage inductance

Fig-8: Basic schematic diagram, dynamic average-value model, and control block diagram of the employed bidirectional dc/dc converter. (a) Basic schematic diagram. (b) Dynamic average-value model. (c) Control block diagram.

The utilization of the two power switches $S1$ and $S2$ can effectively achieve boost or buck mode of operation, while the direction of power flow between the dc microgrid and the battery can also be interchanged [22]. The characteristics of the bidirectional dc/dc converter are different under boost or buck mode of operation. The dynamic average-value model shown in Fig. 4.6(b) [11] is used in this paper, where the switching elements are replaced by a dependent current source and a dependent voltage source to establish a new circuit. Assume that the high-frequency switching phenomena are neglected. To obtain both simple boost mode and buck mode of control, high-frequency pulse width modulation (PWM) must be neglected duty ratio control to achieve bidirectional functions as follows:

$$L_{\text{Battery}}p(i_{\text{Battery}}) = V_{\text{Battery}} - (1 - D_B)V_{\text{DC}}$$
$$- i_{\text{Battery}} \cdot R_{\text{Battery}}$$
$$i_{B\_\text{DC}} = C_{\text{DC}}p(V_{\text{DC}}) = (1 - D_B) \cdot i_{\text{Battery}}$$

$$\text{............ (17)}$$

$$L_{\text{Battery}}p(i_{\text{Battery}}) = D_B \cdot V_{\text{DC}} - V_{\text{Battery}}$$
$$- i_{\text{Battery}} \cdot R_{\text{Battery}}$$
$$i_{B\_\text{DC}} = C_{\text{DC}}p(V_{\text{DC}}) = D_B \cdot i_{\text{Battery}}$$

$$\text{............ (18)}$$

where D_B is the duty ratio of the converter, C_{DC} is the equivalent capacitance of the dc microgrid, L_{Battery} is the external inductance of the battery, R_{Battery} is the internal resistance of the battery, and iBattery and iB_DC are the

currents at the low voltage and high-voltage sides of the converter, respectively. In order to solve the control problem of the bidirectional converter under two different power flow directions, the control strategy is based on an inner current loop control joined with an outer voltage loop control. Fig. 4.6(c) shows the two feedback loops for the battery charging power control and the dc voltage control of the dc microgrid. When disturbances occur, the control of V_{DC} can be achieved by adjusting the battery charging current through feeding back V_{DC} and $P_{Battery}$.

5. RESULTS AND ANALYSIS

This section deals with results and their analysis. The wind and wave systems are designed using MATLAB software. The dynamic changes in torques of wind and wave power generating systems are due to environmental changes in wind speeds on earth surface and on the ocean respectively.
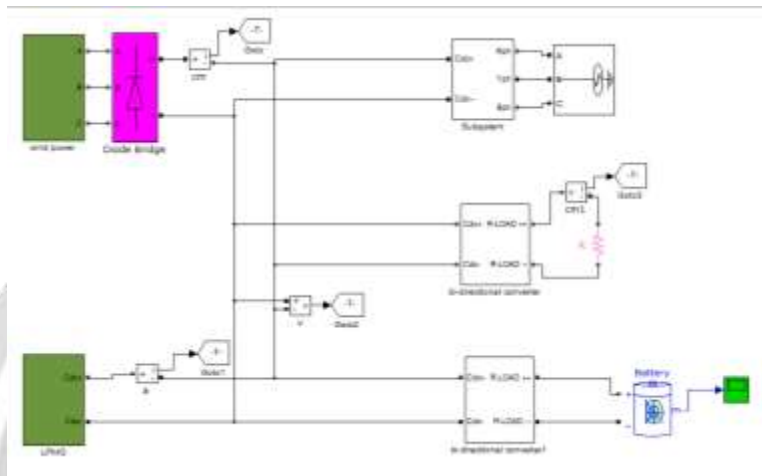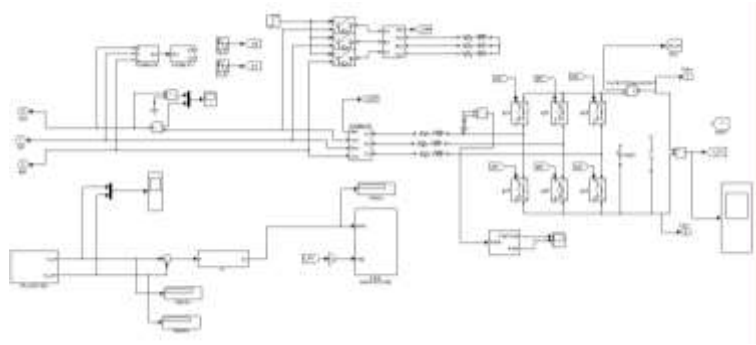

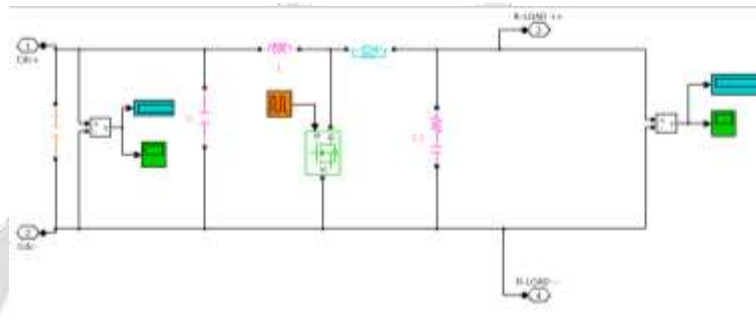**Fig-9:** Simulation block diagram proposed system
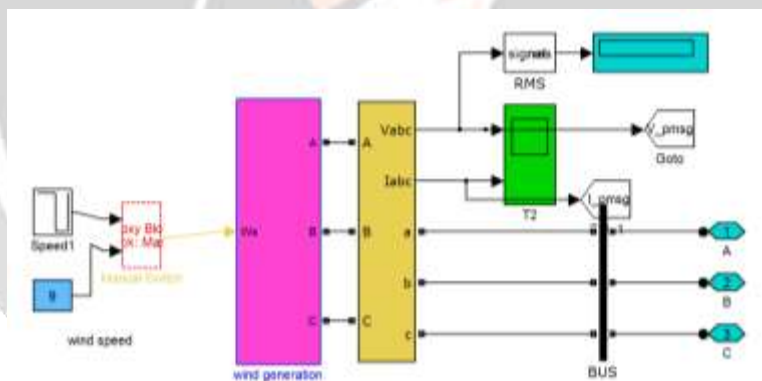
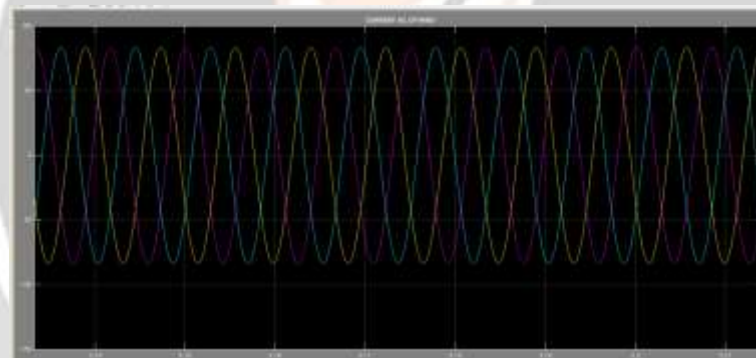**Fig-10:** Simulation block diagram of wind power system
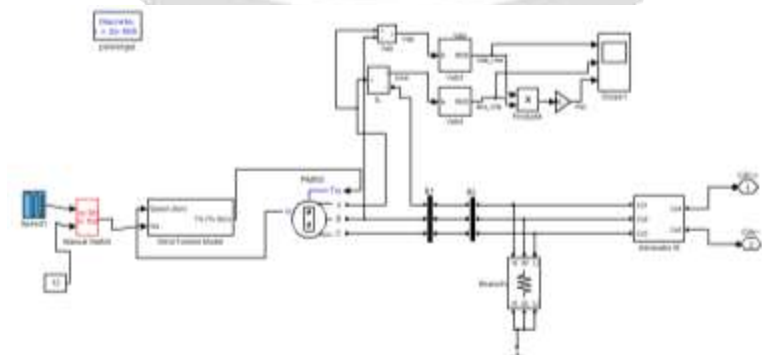
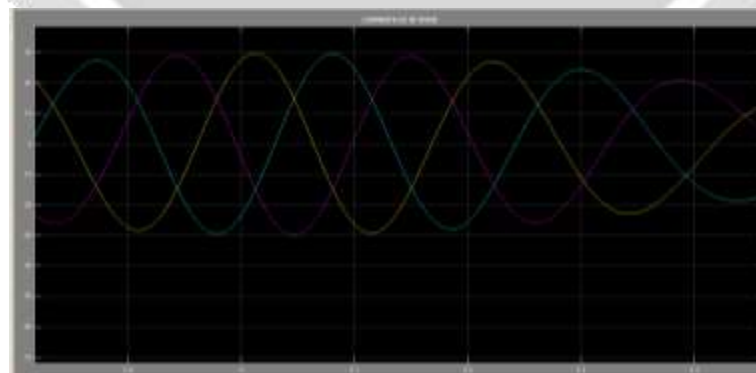**Fig-11:** Simulation block diagram of wave power system

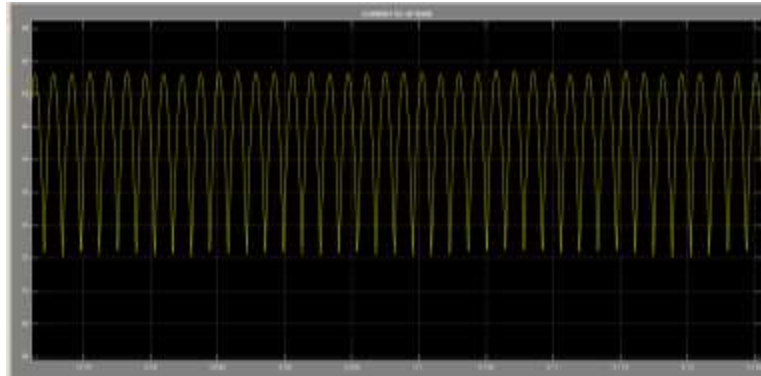**Fig-12:** Simulation block diagram of grid tie invereter system

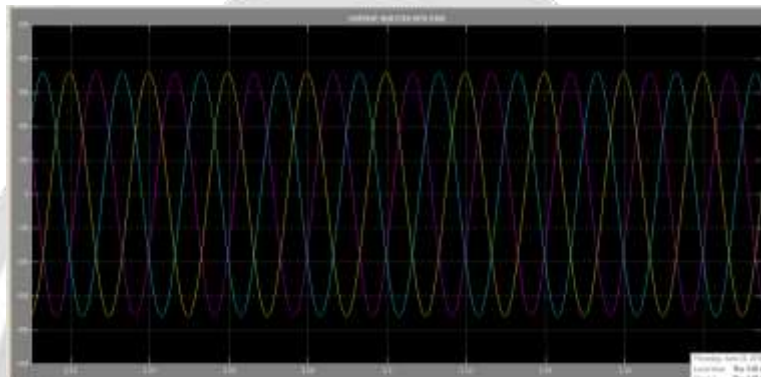**Fig-13:** Simulation block diagram of dc-dc converter

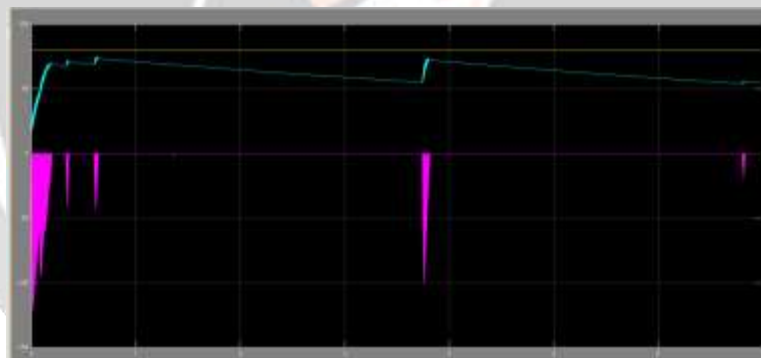**Fig-14:** Simulation block diagram proposed system

Fig-15: Simulation block diagram proposed system

Fig-16: dc-link voltage

Fig-17: three phase grid injected current

Fig-9: soc of battery

6. CONCLUSION

An integration of both wind power and wave power generation systems joined with a dc microgrid has been proposed. A laboratory-grade test system has been presented in this paper to examine the fundamental operating characteristics of the studied integrated system fed to isolated loads using a dc microgrid. For simulation parts, the results of the root-loci plot and the time-domain responses have revealed that the studied integrated system with the proposed dc microgrid can maintain stable operation under a sudden load-switching condition. Comparative simulated and measured results under a load switching have been performed, and it shows that the studied integrated system with the proposed dc microgrid can be operated stably under different disturbance conditions, while both measured and simulated results can match with each other.

7. REFERENCES

[1].   Y. Ito, Y. Zhongqing, and H. Akagi, "DC microgrid based distribution power generation system," in *Proc. 4th IEEE Int. Power Electron. Motion Control Conf.*, 2004, vol. 3, pp. 1740–1745.

[2].   S. K. Kim, J. H. Jeon, C. H. Cho, J. B. Ahn, and S. H. Kwon, "Dynamic modeling and control of a grid-connected hybrid generation system with versatile power transfer," *IEEE Trans. Ind. Electron.*, vol. 55, no. 4, pp. 1677–1688, Apr. 2008.

[3].   C. Abbey and G. Joos, "Supercapacitor energy storage for wind energy applications," *IEEE Trans. Ind. Appl.*, vol. 43, no. 3, pp. 769–776, May 2007.

[4].   X. Liu, P. Wang, and P. C. Loh, "A hybrid ac/dc microgrid and its coordination control," *IEEE Trans. Smart Grid*, vol. 2, no. 2, pp. 278–286, Jun. 2011.

[5].   H. Kakigano, Y. Miura, and T. Ise, "Low-voltage bipolar-type dc microgrid for super high quality distribution," *IEEE Trans. Power Electron.*, vol. 25, no. 12, pp. 3066–3075, Dec. 2010.

[6].   M. G. D. S. Prado, F. Gardner, M. Damen, and H. Polinder, "Modeling and test results of the Archimedes wave swing," *J. Power Energy*, vol. 220, no. 8, pp. 855–868, Dec. 2006.

[7].   B. Das and B. C. Pal, "Voltage control performance of AWS connected for grid operation," *IEEE Trans. Energy Convers.*, vol. 21, no. 2, pp. 353–361, Jun. 2006.

[8].   E. Tara *et al.*, "Dynamic average-value modeling of hybrid-electric vehicular power systems," *IEEE Trans. Power Del.*, vol. 27, no. 1, pp. 430–438, Jan. 2012.

[9].   H. L. Do, "Non-isolated bidirectional zero-voltage-switching dc–dc converter," *IEEE Trans. Power Electron.*, vol. 26, no. 9, pp. 2563–2569, Sep. 2011.

[10].   D. Salomonsson, L. Söder, and A. Sannino, "An adaptive control system for a dc microgrid for data centers," *IEEE Trans. Ind. Appl.*, vol. 44, no. 6, pp. 1910–1917, Nov./Dec. 2008.

[11].   D. Salomonsson and A. Sannino, "Low-voltage dc distribution system for commercial power systems with sensitive electronic loads," *IEEE Trans.Power Del.*, vol. 22, no. 3, pp. 1620–1627, Jul. 2007.

[12].   M. N. Amin and O. A.Mohammed, "DC-bus voltage control technique for parallel-integrated permanent magnet wind generation systems," *IEEE Trans. Energy Convers.*, vol. 26, no. 4, pp. 1140–1150, Dec. 2011.

[13].   T. L. Vandoorn, B. Meersman, L. Degroot, B. Renders, and L. Vandevelde, "A control strategy for islanded microgrids with dc-link voltage control," *IEEE Trans. Power Del.*, vol. 26, no. 2, pp. 703–713, Apr. 2011.

[14].   S. A. Daniel and N. A. Gounden, "A novel hybrid isolated generating system based on PV fed inverter-assisted wind-driven induction generators," *IEEE Trans. Energy Convers.*, vol. 19, no. 2, pp. 416–422, Jun. 2004.

[15].   J. Cao and A. Emadi, "A new battery/ultracapacitor hybrid energy storage system for electric, hybrid, plug-in hybrid electric vehicles," *IEEE Trans. Power Electron.*, vol. 27, no. 1, pp. 122–132, Jan. 2012.

[16].   L. Wang, H.-W. Li, and C.-T. Wu, "Stability analysis of an integrated offshore wind and seashore wave farm fed to a power grid using a unified power flow controller," *IEEE Trans. Power Syst.*, vol. 28, no. 3, pp. 2211–2221, Aug. 2013.